ROYAL SOCIETY OF CHEMISTRY

PAPER

Check for updates

Design of a nanocomposite with gold nanoparticles as the core and casein-templated gold nanoclusters as the shell with ultra-low protein corona for enhanced photodynamic therapy†

Yue Zhang,‡ Yuan Huang,‡ Hao Chen, Xinxin Luo, Jinzhi Zhang, Hangxing Wang, [ID] Qichao Zou* and Suxiao Wang [ID] *

Gold nanoclusters (AuNCs) are well known in biosensing, bio-imaging and drug delivery areas, and they can sensitize the formation of singlet oxygen upon photoexcitation. However, designing AuNCs with a size bigger than 10 nm and in the meantime maintaining the fluorescence property, photodynamic function and long blood circulation time will be a big challenge. Herein, we design a gold nano-composite with gold nanoparticles as the core and casein-templated gold nanoclusters as the shell (AuNPs-CS-AuNCs), having high photodynamic therapy efficiency and ultra-low protein corona properties as demonstrated by *in vitro* and *in vivo* experiments. The protein casein was used as an AuNC preparation template, reducing agent and also as an antifouling agent and their ultra-low protein corona properties are better than those of conventional PEGylated or BSA-coated nanocomposites. The photodynamic therapy efficiency of AuNPs-CS-AuNCs can be well enhanced by the synergy effect of CS-AuNCs and AuNPs which is due to the surface plasmonic amplification and energy transfer from AuNPs in the core to neighboring AuNCs on the shell for enhanced reactive oxygen species formation. Moreover, the size of our gold nanocomposites, around 31 nm, is bigger than that of conventional AuNCs, facilitating cell membrane crossing. The AuNPs-CS-AuNCs we designed can be potentially used as an anti-cancer therapy agent with excellent antifouling properties and high photodynamic therapy efficiency.

Introduction

Gold nanoclusters (AuNCs) are ultra-small gold nanoparticles (AuNPs), with diameters smaller than 5 nm, which are composed of a few gold atoms, and AuNCs are more like "artificial atoms".[1,2] Unlike conventional bulk gold nanocomposites (gold nano-particles, gold nanorods, *etc.*), the gold nanoclusters possess a strong quantum confinement effect of free electrons in the particles and the continuous density turns into discrete energy levels, leading to unique molecule-like properties.[3] Therefore, AuNCs possess superior physical and chemical properties like

Ministry of Education Key Laboratory for the Synthesis and Application of Organic Functional Molecules, Hubei Collaborative Innovation Centre for Advanced Organic Chemical Materials, College of Chemistry and Chemical Engineering, Hubei University, Wuhan, 430062, China. E-mail: wsx@hubu.edu.cn, zouqichao85@sina.com

enhanced catalyst activity and intense photoluminescence with high quantum yields, facilitating their wide application in biosensing, bio-imaging and drug delivery due to their attractive features.[4] Moreover, AuNCs are known to sensitize the formation of singlet oxygen upon photoexcitation and exert a nucleus-targeting nanomaterial-mediated photodynamic ther-apy (PDT) effect on cancer cell killing without the co-presence of any organic photosensitizer.[5–8]

To prepare the AuNCs, the template method is the typical "Top-Up" method for controlling the size and the Au^{3+} ions are reduced to Au^0 by suitable reducing agents. Proteins such as BSA,[9] transferrin,[10] trypsin[11] and lysozyme[12] are usually used as templates to prepare AuNCs as reducing agents and also stabilizers, which has multiple advantages including green synthesis, biocompatibility, and high water solubility.[13–15] Casein with excellent biocompatibility, biodegradability, and pH-responsive structural and thermal stability has been widely used for drug delivery systems.[16,17] Casein has multiple amino acid residues with 19.5% of amine-containing amino acids

(similar to BSA with 19.1%), which is responsible for the Au ion uptake and reduction, potentiating it to become a good candidate as a template for AuNC preparation.[14] Moreover, casein contains sulfur-bearing amino acids, which can be functionalized as nanoparticle thiol-capping agents, leading to strong Au–S interactions on the NC surface. Casein also has strong reducing agent amino acids such as tryptophan and strong metal binding amino acids like histidine.[18] In addition, we previously demonstrated that the casein coated nanoparticle has an excellent antifouling property (ultra-low protein corona) due to the high interaction energy of the casein–serum protein pair and the small number of hydrogen bond formations between them.[19] The antifouling properties of nanoparticles will avoid the deposition of complement proteins on the surfaces, which could avoid inducing strong complement activation and extend the blood circulation time.[20]

Although the ultrasmall AuNCs have many advantages for biological applications, the enthalpic limit for a spherical nanoparticle occurs at a size of about 30 nm, indicating that nanoparticles smaller than this limit will not be able to drive the membrane-wrapping process effectively.[21] However, indeed, the nanoparticles larger than 60 nm in diameter result in a receptor shortage, which decreases the uptake because of the increasing entropic penalty, and most *in vitro* studies show a maximum cellular uptake within the 10–60 nm range.[22–24] In addition, in terms of blood circulation time, the nanoparticles with a diameter less than approximately 10 nm will be rapidly eliminated by the kidneys through renal clearance.[25,26] Hence, the size of AuNCs is too small to be used as a nanodrug for anti-cancer therapy and the size in the range of 30–60 nm will be ideal. However, a nanoparticle with larger sizes will activate the complement system, leading to quick removal from the blood stream and accumulation in the liver and spleen.[27,28] Moreover, it is difficult to sustain the fluorescent properties of AuNCs when their sizes are over 10 nm, and this phenomenon may limit their potential applications.[29,30] Therefore, designing AuNCs with a size bigger than 10 nm and in the meantime maintaining the fluorescence property, photodynamic function and long blood circulation time will be needed.

Herein, to address this issue, we design core–shell AuNCs with AuNPs as cores (AuNPs-CS-AuNCs), which can not only maintain the fluorescence properties and photodynamic therapy function but also maintain the size around 31 nm, which is bigger than conventional AuNCs, facilitating cell membrane crossing, and have the ultra-low protein corona properties with potentially long blood circulation time by using protein casein as the AuNC preparation template, reducing agent and also as an antifouling agent. The PDT efficiency of core–shell AuNPs-CS-AuNCs can be well enhanced by the AuNPs as the core material due to surface plasmonic amplifying the photonic energy absorption and energy transfer from AuNPs in the core to neighboring AuNCs on the shell for enhanced reactive oxygen species formation. Therefore, the synergy effect of CS-AuNCs and AuNPs in our gold nanocomposite provides an appropriate size range and superior PDT efficiency and the casein on the shell provides an ultralow protein corona effect compared to conventional PEGylated or BSA-coated gold nanocomposites. Our work opens a new avenue to design gold nanoclusters with high photodynamic therapy efficiency and ultra-low protein corona properties for cancer therapy.

Methods

Materials

Casein and tetrachloroauric(III) acid (HAuCl$_4$·3H$_2$O) were purchased from Macklin. Trisodium citrate (C$_6$H$_5$Na$_3$O$_7$·2H$_2$O) (AR), sodium hydroxide (AR), dimethylformamide (AR), acetic acid (AR) and 1,3-diphenylisobenzofuran (DPBF, AR) were purchased from Aladdin. Fetal bovine serum (FBS) was purchased form HyClone.

Synthesis of gold nanoparticles (AuNPs)

A typical chemical reduction method for gold nanoparticle synthesis was applied here.[31] Briefly, 50 mL of HAuCl$_4$ aqueous solution was heated to boiling and 1 mL of trisodium citrate was added under vigorous stirring. The color of the solution turned light blue and then changed to brilliant red after 10 minutes, indicating the formation of AuNPs. Then, the synthesized AuNP solution was cooled at room temperature.

Synthesis of PEGylated AuNPs

The nanoparticles were PEGylated using thiol functionalized methoxy-poly(ethylene-glycol) (mPEG-SH), with 1000 Da average molecular weight. In detail, 100 mg PEG-SH was dissolved in 1 mL MilliQ water in an ultrasonic bath by avoiding heating of the sample. This solution was added quickly to 20 mL of the citrate-stabilized gold nanoparticle solution prepared above and gently stirred for 3 hours. The PEGylated nanoparticles were cleaned by centrifugation and redispersion in water.

Synthesis of casein-templated gold nanoclusters (CS-AuNCs)

A typical synthesis method of protein–templated gold nanoclusters was applied here.[9] 0.1 g casein with 20 mL 0.01 mol L^{-1} phosphate buffer solution (PBS) was boiled for 10 min until completely dissolved and denatured. The solution was cooled to room temperature. Then, 6 mL of the as-prepared casein solution and 4 mL PBS solution were added into a flask with vigorous stirring. pH was adjusted by dropping NaOH solution (1 mol L^{-1}) to 12. The mixture was under continuous stirring for 10 mins. Then, 64 μL of HAuCl$_4$ aqueous solution (0.254 mol L^{-1}) was added. The mixture was further incubated at 45 °C for 6 h. The AuNCs were purified by centrifugation under 10 000 rpm for 10 min and stored at 4 °C.

Synthesis of the core–shell nanocomposite AuNPs-CS-AuNCs and AuNPs-BSA-AuNCs

The core–shell AuNPs-CS-AuNCs was prepared from the reduction of Au atoms entrapped by the casein coated on the surface of AuNPs. In detail, 5 mL of the purified as-prepared AuNPs was mixed with 13 mL casein aqueous solution (0.3 mg mL^{-1}) with incubation at 37 °C for 6 h to obtain casein-coated Au NPs. The extra casein was eliminated by centrifugation at 12 000 rpm

for 30 min and the casein coated AuNPs were resuspended in PBS buffer. Then, pH was adjusted by dropping NaOH solution (1 mol L^{-1}) to 12 under stirring for 10 min, and 42 μL of HAuCl$_4$ aqueous solution (0.254 mol L^{-1}) was added. The mixture was further incubated at 45 °C for 6 h. The AuNPs-CS-AuNCs was purified by centrifugation under 10 000 rpm for 10 min and stored at 4 °C for further use. By applying bovine serum albumin (BSA) instead of casein and keeping the procedures all the same, the AuNPs-BSA-AuNCs were prepared.

Characterization

Dynamic light scattering (DLS) and zeta potential measurements were carried out using a Zetasizer Nano ZS system (Malvern Instruments, Ltd., UK). DTS Application 5.10 software was employed to analyze the data obtained. The size and shape of the NPs were also measured by high-resolution transmission election microscopy (HRTEM) (TEM-2100PLUS HRTEM, JEOL, Japan). The chemical groups of the nanoparticles were analyzed by Fourier transform infrared (FTIR) (Thermo NICOLET iS10) in transmission mode. For that, dried material powders were mixed with KBr (40 mg) and then formed into a disc in a manual press. Transmission spectra were recorded using at least 32 scans with 4 cm^{-1} resolution in the spectral range 4000–400 cm^{-1}. X-Ray photoelectron spectroscopy (XPS) studies were conducted by using an instrument VGMultilab of JEOL Ltd. Structural characterization of the as-prepared nanocomposite was carried out using room temperature powder X-ray diffraction (XRD) performed on a Bruker D8 Advance diffractometer. The target used was CuKα radiation at a scan rate of 10° min^{-1}. UV-Vis absorption spectra were acquired using a double-beam spectrophotometer TU-1901. Photoluminescence spectra were acquired using an F-4600 (Hitachi) spectrometer. The sodium dodecyl sulfate polyacrylamide gel electrophoresis (SDS-PAGE) method was also used to determine the existence of casein on the nanocomposite. The nanoparticle-casein complex was separated and denatured by boiling for 5 min in loading buffer (Coolaber 3 × protein loading buffer with DTT), and then separated by size in the moiety of porous 10% polyacrylamide gel (1D SDS-PAGE), in an electric field using a Mini-PRO4 electrophoresis system from WIX. The electrophoresis was run under a constant voltage (120 V, 80 min). The gels were stained using silver stain (Beyotime) for 2 h, followed by destaining overnight in deionized water.

Protein corona property determination

Dynamic light scattering (DLS) was applied to compare the sizes of nanoparticles before and after incubation with the FBS solution.

Singlet oxygen detected by DPBF

The generated singlet oxygen under light irradiation is detected by a highly efficient singlet oxygen scavenger 1,3-diphenyliso-benzofuran (DPBF). In detail, 5 mg of DPBF was dissolved into 1 mL of dimethyl formamide (DMF) to make DPBF solution (5 mg mL^{-1}). Then, 4 μL of the prepared DPBF solution and 100 μL of AuNPs or CS-AuNCs or AuNPs-CS-AuNCs were added

into 3 mL of DMF and exposed to 570 nm irradiation light for 0, 30, 60, 90, 120, 150, 180, 210, 240 and 270 s, respectively. The absorption spectra were measured and the absorbance (λ = 419 nm) decrease was recorded. Moreover, the absorption spectra of pure DPBF solution with light irradiation and DPBF/ NP mixture without light irradiation were all recorded to exclude the interference of DPBF and spectrometer.

Cytotoxicity and phototoxicity of gold nanocomposites: cell viability by MTT assay

The cytotoxicity and phototoxicity of the as-prepared gold nanocomposites against the HeLa cells were assayed by the MTT assay (3-(4,5-dimethyl-2-thiazolyl)-2,5-diphenyl-2H-tetra-zolium bromide) (Sigma Aldrich). In detail, HeLa cells were collected and seeded onto 96-well plates at 5 × 10^4 cells per well. After overnight culture for 24 h, the AuNPs, CS-AuNCs and AuNPs-CS-AuNCs were separately added to the cells and incubated for another 24 h at 37 °C. Then, after another 24 h of incubation, the cells were washed twice with PBS buffer to remove any noninternalised NPs. Then, the cytotoxicity was derived by the MTT assay. In terms of phototoxicity, the gold nanocomposite-treated HeLa cells were under irradiation for different time points and incubated for another 24 hours, and then, the cell viability was measured by the MTT assay. The concentration of gold nanocomposites was used as 0.03 mM.

In vivo photodynamic therapy

HeLa cells were subcutaneously injected into the BALB/c mice, and when the tumors reached 100 mm^3, PBS as a blank, AuNPs, CS-AuNCs and AuNPs-CS-AuNCs were separately administered into the mice every four days followed by 5 mins of white light irradiation each time. The treatment was provided for 19 days, and the tumor weights were recorded every two days. When the treatment was finished, the tumors were collected for histo-logical analysis. All of the animal experiments were carried out in accordance with the relevant laws and guidelines issued by the Ethical Committee of Hubei University and were in agree-ment with the guidelines of the Institutional Animal Care and Use Committee.

Results and discussion

The citrate-stabilized AuNPs are prepared by a typical single-phase aqueous reduction of tetrachloroauric acid (HAuCl$_4$) by sodium citrate. AuNCs were prepared by a typical protein templated reduction method by applying casein as the scaffold and activating the casein reduction at pH 12. The as prepared CS-AuNCs were stabilized within casein molecules as casein–AuNC bioconjugates. As shown in Fig. 1(a), the core–shell gold nanoclusters with gold nanoparticles as cores (AuNPs-CS-AuNCs) were prepared by decorating AuNPs by casein and reducing Au ions to form AuNCs on the shell of AuNPs. The hydrodynamic diameters of AuNPs and CS-AuNCs were 16 nm and 3.5 nm, respectively, and the core–shell AuNPs-CS-AuNCs was much larger than those two, at 31.0 nm (Fig. 1(b)–(d)).
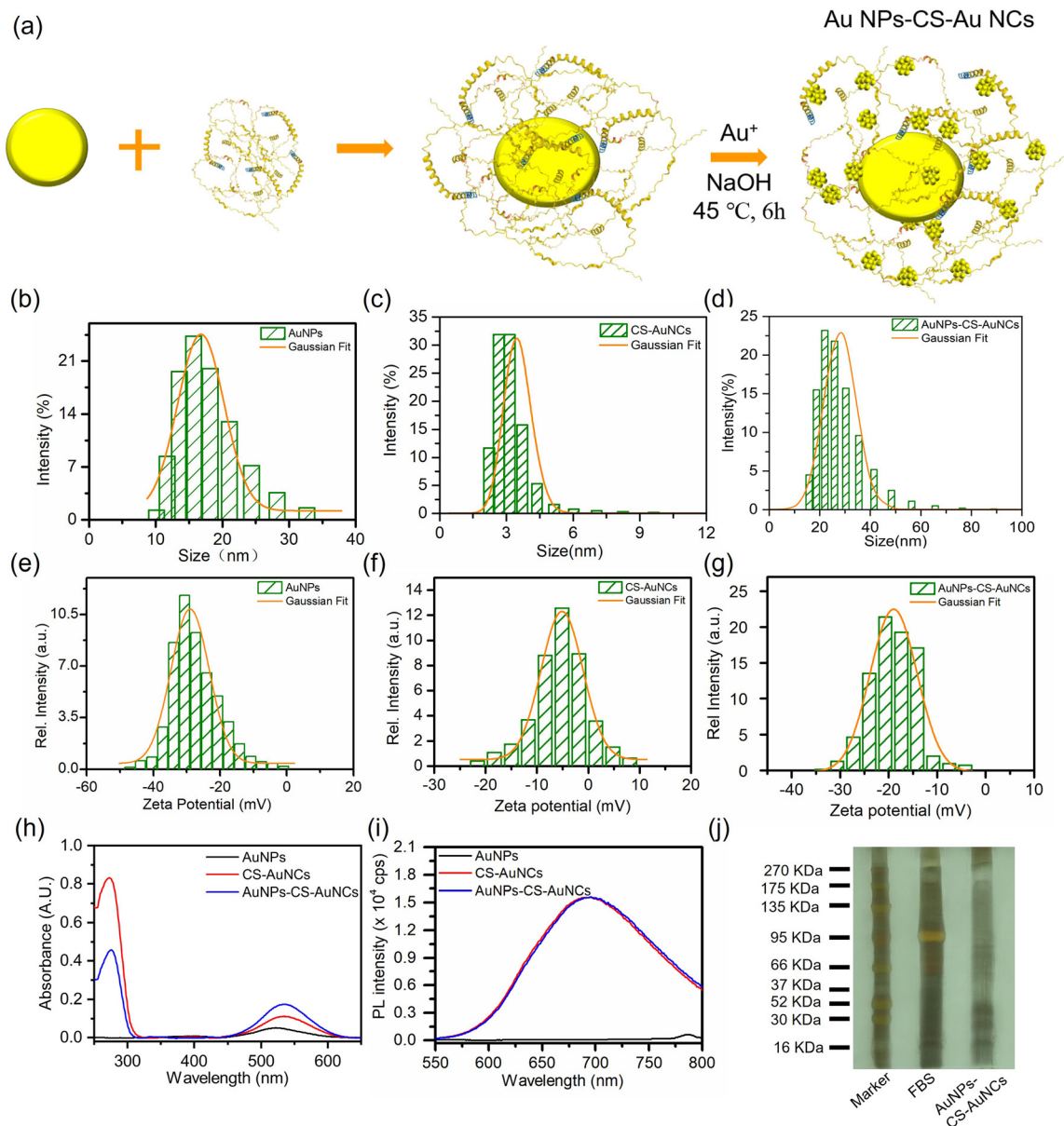
Fig. 1 (a) Schematic of the preparation of core–shell AuNPs-CS-AuNCs. Hydrodynamic diameters (b)–(d) and zeta potentials (e)–(g) of AuNPs, CS-AuNCs and AuNPs-CS-AuNCs. (h) Absorption and (i) emission spectra of AuNPs, CS-AuNCs and AuNPs-CS-AuNCs. (j) Protein bands from SDS-PAGE of AuNPs-CS-AuNCs.

The shell thickness can be estimated by comparing the size of AuNPs (16 nm) and AuNPs-CS-AuNCs (31 nm) from DLS to be 15 nm. As shown in Fig. 1(e)–(g), the zeta potential on the surface of AuNPs was −30 mV, which was due to the citrate at the surface of AuNPs as the stabilizer, indicating their high colloidal stability. A higher zeta potential of CS-AuNCs of −5 mV was observed, owing to the casein as the scaffold on the CS-AuNCs. And the zeta potential of core–shell AuNPs-CS-AuNCs of −20 mV was attributed to the combination of citrate and casein, confirming the casein as the bridge to connect AuNPs and AuNCs and the successful preparation of core–shell AuNPs-CS-AuNCs. Moreover, these three types of gold nanocomposites exhibit excellent colloidal stability in deionized water for more than 30 days (Fig. S1, ESI†).

Typical plasmonic absorption at 522 nm was observed for AuNPs with consistence of the AuNPs with the size at 16 nm, as shown in Fig. 1(h) (black line). For CS-AuNCs, the absorption at 278 nm was attributed to aromatic residues such as trypto-phan, tyrosine and disulfide bonds in casein as shown in Fig. 1(h) (red line).[32] A lower energy peak at 535 nm is attributed to sp to sp and d to sp transition which is consistent with the absorption spectrum of 25 gold atom nanocluster.[9,33] The core–shell AuNPs-CS-AuNCs exhibited the absorption maxi-mum at 278 nm, which was attributed to casein, and the 3 nm blue shift of the absorption peak at 532 nm compared to the pure CS-AuNCs (535 nm) is due to the overlapping of AuNPs and AuNCs. The absorbance at 532 nm is also the addition of

AuNPs and AuNCs, indicating the successful preparation of the core–shell AuNPs-CS-AuNCs. Under 525 nm irradiation, negligible emission was observed for AuNPs, while the photoluminescence spectrum of CS-AuNCs and AuNPs-CS-AuNCs showed a main peak at 694 nm (Fig. 1(i)), corresponding to the emission of the 25 Au atom composed AuNCs.[9,33] By only excitation at AuNC absorption maximum wavelength (278 nm), the fluorescence quantum yields (PLQY) of CS-AuNCs and core–shell AuNPs-CS-AuNCs were similar, 3.06% and 2.73%, respectively. However, the PLQYs of CS-AuNCs and AuNPs-CS-AuNCs by excitation at 532 nm were 30.20% and 57.26%, respectively. The much higher PLQY for AuNPs-CS-AuNCs than CS-AuNCs (532 nm excitation) confirms the surface plasmonic amplifying the photonic energy absorption and energy transfer from AuNPs to neighboring AuNCs. To further demonstrate the presence of casein on the core–shell AuNPs-CS-AuNCs, it was analysed by sodium dodecyl sulfate-polyacrylamide-gel electrophoresis (SDS-PAGE) with protein markers and FBS solution as standard indicators. Very pronounced protein bands were shown for AuNPs-CS-AuNCs, confirming that the casein was coated on the shell of AuNCs, as shown in Fig. 1(j). These results also indicate the successful preparation of core–shell AuNPs-CS-AuNCs.

High resolution transmission electron microscopy (HR-TEM) was applied to directly observe the morphology of the as-prepared
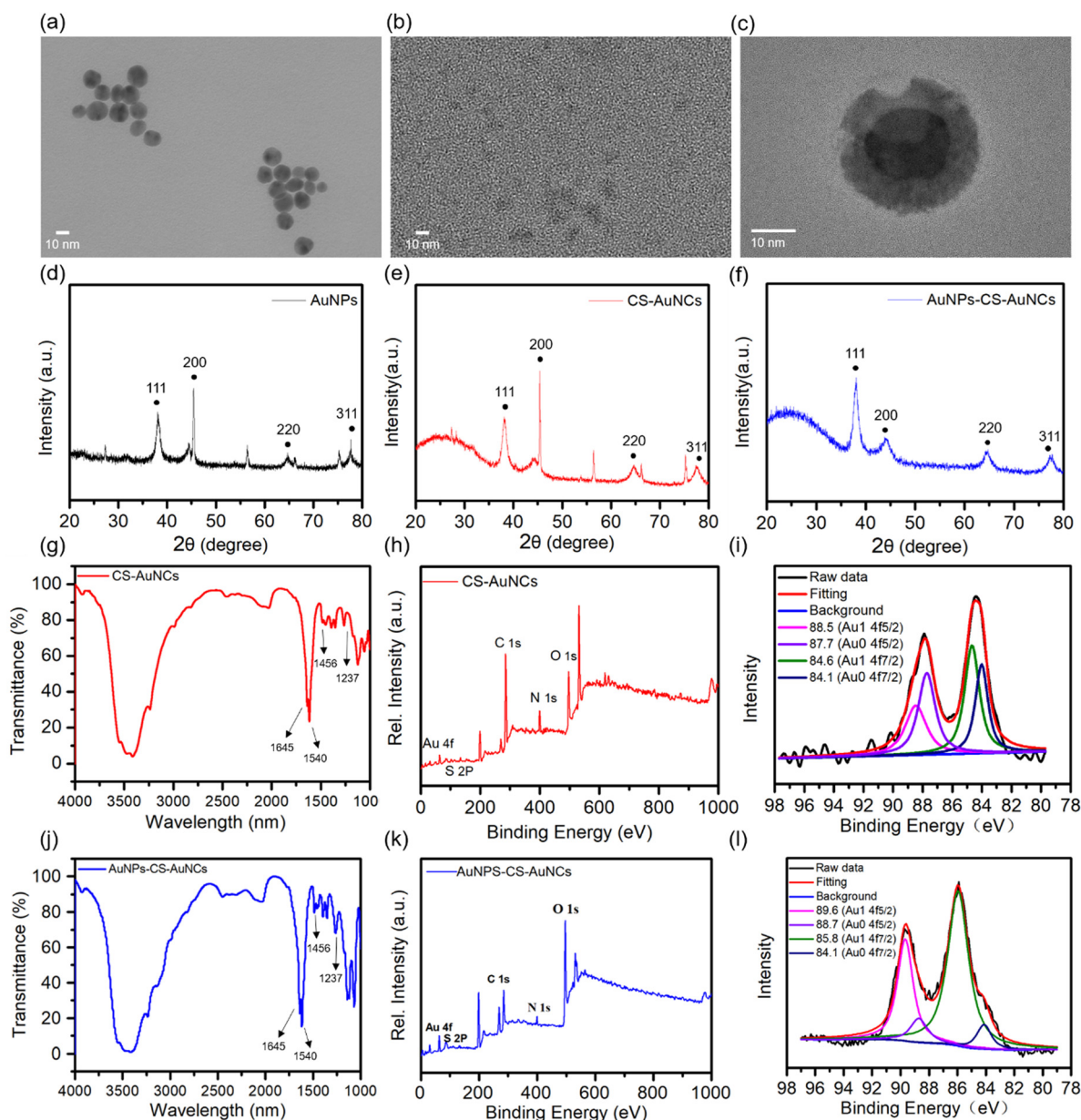

Fig. 2 HR-TEM images of (a) AuNPs, (b) CS-AuNCs and (c) AuNPs-CS-AuNCs. (d)–(f) XRD spectrum of (d) AuNPs, (e) CS-AuNCs and (f) AuNPs-CS-AuNCs. (g) FTIR spectrum of CS-AuNCs. (h) XPS spectrum of CS-AuNCs. (i) Au 4f XPS spectrum of CS-AuNCs. (g) FTIR spectrum of AuNPs-CS-AuNCs. (h) XPS spectrum of AuNPs-CS-AuNCs. (i) Au 4f XPS spectrum of AuNPs-CS-AuNCs.

gold nanocomposite. AuNPs and CS-AuNCs have a spherical shape with the size at 16 nm and 4 nm, respectively (Fig. 2(a) and (b)). The core–shell structure can be estimated by the TEM images of AuNPs-CS-AuNCs from Fig. 2(c). XRD patterns of AuNPs show that the characteristic diffraction peaks are at 38° and 45°, corresponding to lattice faces (111) and (200) and the two peaks at 65° and 75° correspond to diffraction indices (220) and (311), which are a typical pure Au face-centered cubic (fcc) phase (Fig. 2(d)).[34] In addition to the above typical four diffraction index peaks, XRD patterns of CS-AuNCs and core–shell AuNPs-CS-AuNCs exhibited a broad dispersion peak in the range of 15–35° which is attributed to the amorphous structure of casein (Fig. 2(e) and (f)), demonstrating the protein coated gold crystal structure. Moreover, the relatively weaker and wider (200) peak at 45° for AuNPs-CS-AuNCs indicates the smaller AuNCs on the shell of the gold nanocomposite.[35]

In addition, the FTIR spectrum of AuNPs-CS-AuNCs is shown in Fig. 2(g). The bands centred at 1645 cm^{-1} (C=O stretching), 1540 cm^{-1} (N–H bending) and 1237 cm^{-1} (C–N stretching) are attributed to the amide group of casein.[36,37] The weak peak at 1456 cm^{-1} corresponds to the formation of the S–Au bond.[38] A similar FTIR spectrum was observed for AuNPs-CS-AuNCs as shown in Fig. 2(j). X-ray photoelectron spectroscopy (XPS) was subsequently used to characterize the in-depth chemical states of CS-AuNCs and AuNPs-CS-AuNCs. As shown in Fig. 2(h) and (k), there are five elements of Au, S, C, N, and O on both CS-AuNCs and AuNPs-CS-AuNCs. The presence of S, C, N and O indicates the protein casein involved in the materials as the template. According to Fig. 2(i) and (l), the XPS spectrum of Au 4f confirmed the presence of two different doublets of Au 4f$_{7/2}$, one at 84.1 eV and the other at 84.6 eV corresponding to Au(0) and Au(I), respectively. Another XPS peak assigned to
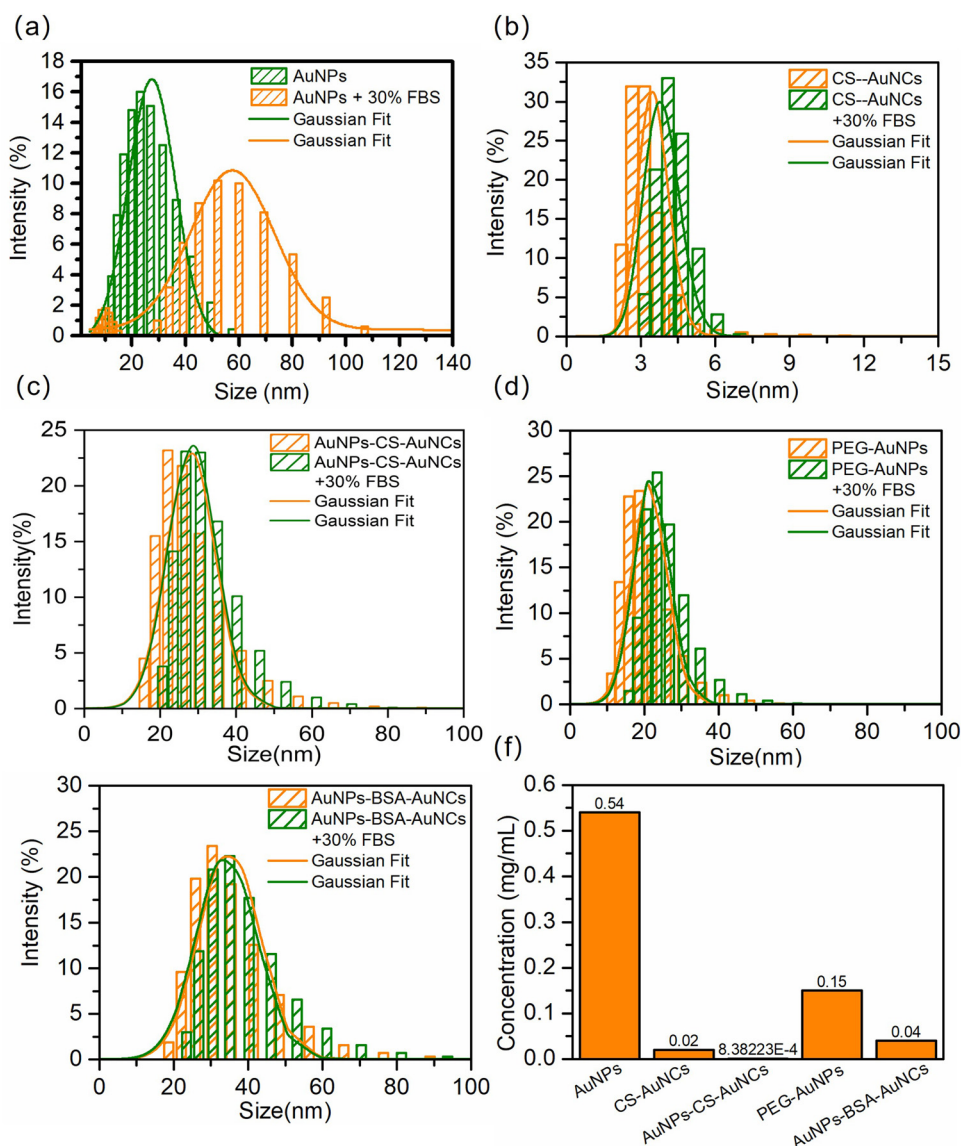

Fig. 3 Hydrodynamic diameters of (a) AuNPs, (b) CS-AuNCs, (c) AuNPs-CS-AuNCs, (d) PEG-AuNPs and (e) AuNPs-BSA-AuNCs before (blue) and after (orange) 30% FBS incubation. (f) Protein corona quantification on each type of NP.

Au$_{5/2}$ was located at 88.7 eV and 89.6 eV which was also assigned to Au(0) and Au(ɪ), respectively.[10] These demonstrated a compositional mixture of a Au(0) core with surface Au(ɪ) atoms. However, the percentage ratio of Au(1) at the 4f$_{5/2}$ state for AuNPs-CS-AuNCs is *ca.* 77% which is much higher than that of CS-AuNCs at *ca.* 42%, indicating the formation of core shell

protein templated AuNPs-CS-AuNCs. The C 1s, N 1s and O 1s spectra are shown in Fig. S2 (ESI†).

To determine the interaction of the NPs with proteins in the serum environment, the NPs were separately incubated with 30% fetal bovine serum (FBS) for 1 h. AuNPs show a pronounced 35 nm-enhancement in mean diameter and much
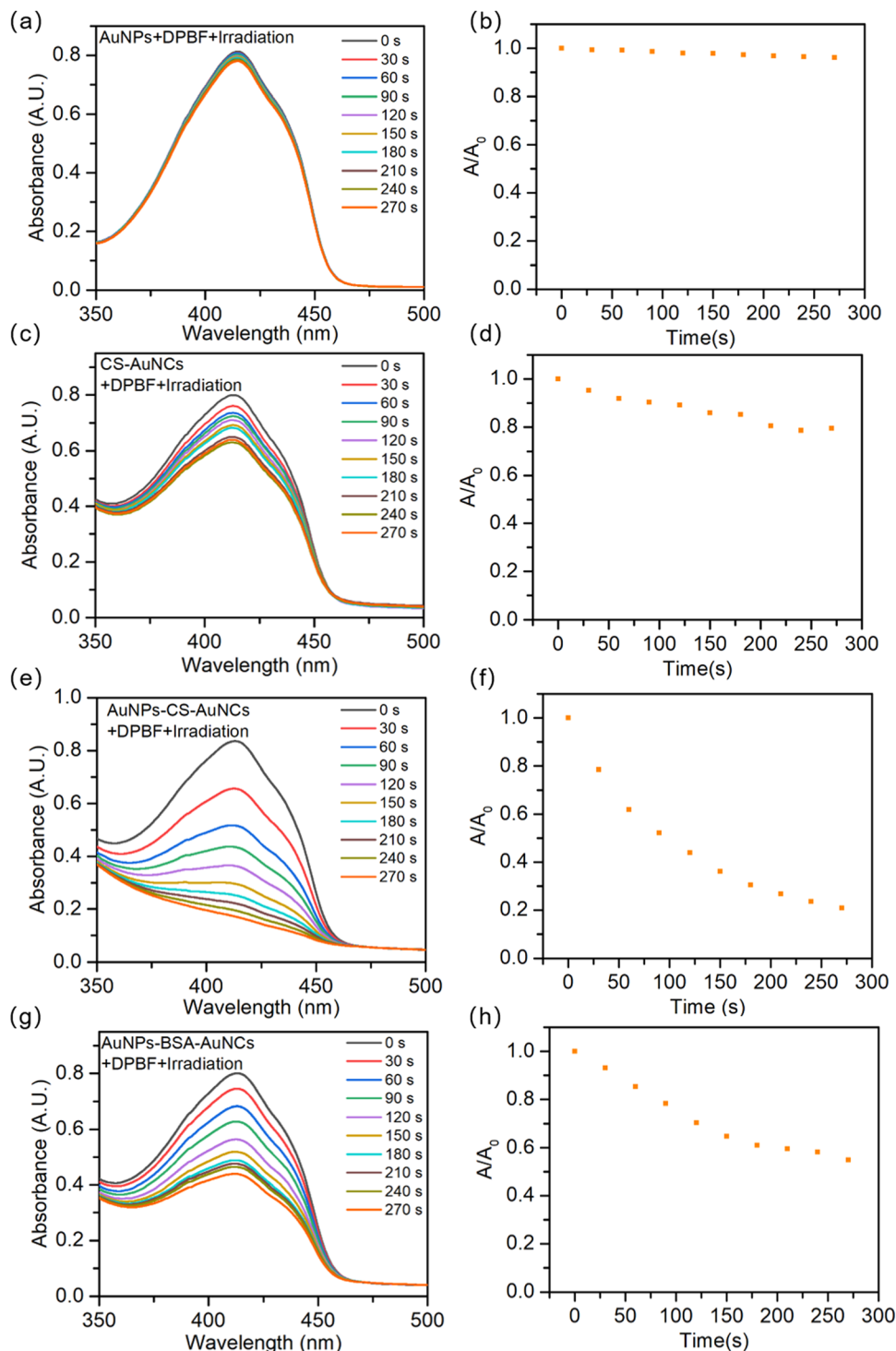
Fig. 4 Absorption spectra of DPBF under 570 nm irradiation at different times and absorbance ratio of the irradiation time maximum absorbance (At) to the time zero maximum absorbance (A0) for (a), (b) AuNPs, (c), (d) CS-AuNCs, (e), (f) AuNPs-CS-AuNCs and (g), (h) AuNPs-BSA-AuNCs.

broader distribution (Fig. 3(a)), indicating their NP–protein complex (protein corona) formation. However, almost no size differences for CS-AuNCs and AuNPs-CS-AuNCs under 30% FBS incubation were observed, as shown in Fig. 3(b) and (c), which indicates the ultra-low protein corona for CS-AuNCs and AuNPs-CS-AuNCs due to the protection of casein coating. For comparison, PEGylated gold nanoparticles (PEG-AuNPs) and BSA protein coated core–shell NPs (AuNPs-BSA-AuNCs) were also prepared and incubated with 30% FBS. No obvious diameter changes were observed for them (Fig. 3(d) and (e)). To further demonstrate the antifouling properties of synthesized NPs, the concentration of protein corona per unit volume of each sample was measured by the BCA (bicinchoninic acid) method. The NP concentration was also controlled by the gold ion and the amount of precoated casein was subtracted from the total mass of protein detected. As shown in Fig. 3(f), the largest amounts of proteins adsorbed on AuNPs were observed and nearly 27 times less amount of protein for CS-AuNCs and negligible amount of proteins for AuNPs-CS-AuNCs were observed. In comparison, the PEG-AuNPs indeed show 3.6 times less amount of protein corona than pure AuNPs, but still much higher than CS-AuNCs and AuNPs-CS-AuNCs. Moreover, although AuNPs-BSA-AuNCs exhibited 3.75 times amount of protein less than that of PEG-AuNPs, it is still much higher than that of CS-AuNCs and AuNPs-CS-AuNCs. These results demonstrate the superior antifouling properties of AuNPs-CS-AuNCs and it exhibits much better antifouling capability than conventional PEGylation and BSA decoration. Therefore, casein not only acts as an AuNC preparation template, but also protects the NPs out of protein corona as an antifouling agent.

Furthermore, to investigate the photodynamic therapy properties of these gold nanocomposites, the generated singlet oxygen under light irradiation is detected by a highly efficient singlet oxygen scavenger 1,3-diphenylisobenzofuran (DPBF). A solution mixture of DPBF and AuNPs or CS-AuNCs or AuNPs-CS-AuNCs was exposed to 390 nm irradiation light, in which DPBF was consumed directly by the generated singlet oxygen, which was monitored by the decrease in absorbance ($\lambda = 419$ nm). As shown in Fig. S3a (ESI†), the impact on DPBF excitation was eliminated by directly exciting DPBF only and no absorbance decrease was observed under illumination. For the solution mixture of NPs with DPBF without illumination, no absorbance decrease was observed as shown in Fig. S3b–d (ESI†), eliminating the impact of measurements from an absorption spectrometer. As shown in Fig. 4(a) and (b), the absorbance of DPBF shows no changes with the increase in irradiation time for AuNPs, indicating that no photodynamic therapy function was achieved for AuNPs. A 20% absorbance decrease was observed after 270 s of irradiation for CS-AuNCs, while more than 80% absorbance decrease of DPBF was observed for AuNPs-CS-AuNCs (Fig. 4(c) and (f)). The much more pronounced absorbance decrease suggests the better singlet oxygen generation function and higher photodynamic therapy efficiency for the core–shell AuNP-coated AuNC structure, which could be because the AuNPs as the core material with superior surface plasmonic properties may amplify photonic energy absorption
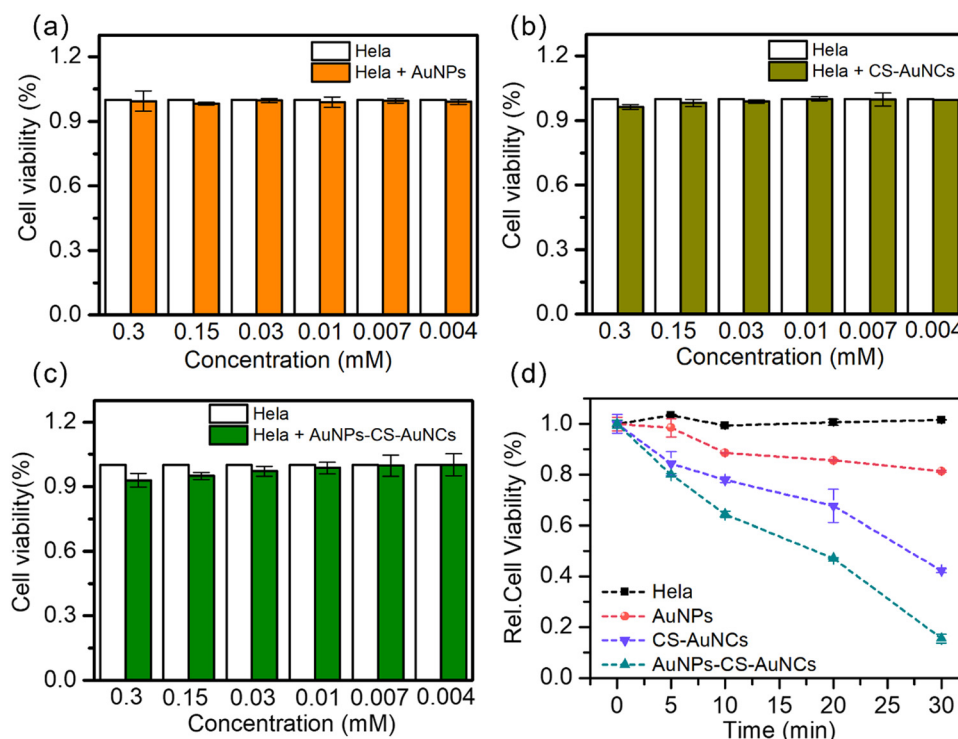

Fig. 5 Cytotoxicity of (a) AuNPs, (b) CS-AuNCs and (c) AuNPs-CS-AuNCs at different concentrations (gold atom concentration) after 24 h of incubation with HeLa cells. (d) Cell viability of HeLa cells incubated with AuNPs, CS-AuNCs and AuNPs-CS-AuNCs with the concentration at 0.03 mM under different irradiation times.

and then transfer the energy to neighboring AuNCs on the shell for enhanced reactive oxygen species (ROS) formation.[39,40] For comparison, as shown in Fig. 4(g)–(h), the singlet oxygen efficiency of AuNPs-BSA-AuNCs was also investigated and more than 48% decrease was observed, which is still much higher than that of CS-AuNCs, indicating the advantage of the core–shell structure. Moreover, the much higher efficiency of AuNPs-CS-AuNCs than AuNPs-BSA-AuNCs might be due to the assistance of casein in the energy transfer system.

To further demonstrate the cytotoxicity and photodynamic efficiency of our gold nanocomposite, *in vitro* studies were applied. As shown in Fig. 5(a)–(c), the AuNPs, AuNCs and AuNPs-CS-AuNCs showed non-cytotoxicity in terms of the viability of HeLa cells after 24 h of incubation with various

NP concentrations from 0.3 M to 0.04 M. Then, the viability of HeLa cells incubated with gold nanocomposites under 570 nm irradiation light was detected by the MTT assay, as shown in Fig. 5(d). The viability of HeLa cells as a blank decrease less than ±1%, indicating that direct damage by light irradiation to the cells is limited. Similar to the blank sample, a negligible cell damage of the AuNP treated group was observed, indicating the non-singlet oxygen release. About 56% viability decrease was observed for CS-AuNCs, while an 88% decrease was observed for AuNPs-CS-AuNCs after 30 min of irradiation. These results demonstrate that the comparable more efficient cell damage under light irradiation for AuNPs-CS-AuNCs may also be due to the surface plasmonic enhancement of AuNPs. In addition, better cell penetration for AuNPs-CS-AuNCs with a larger size
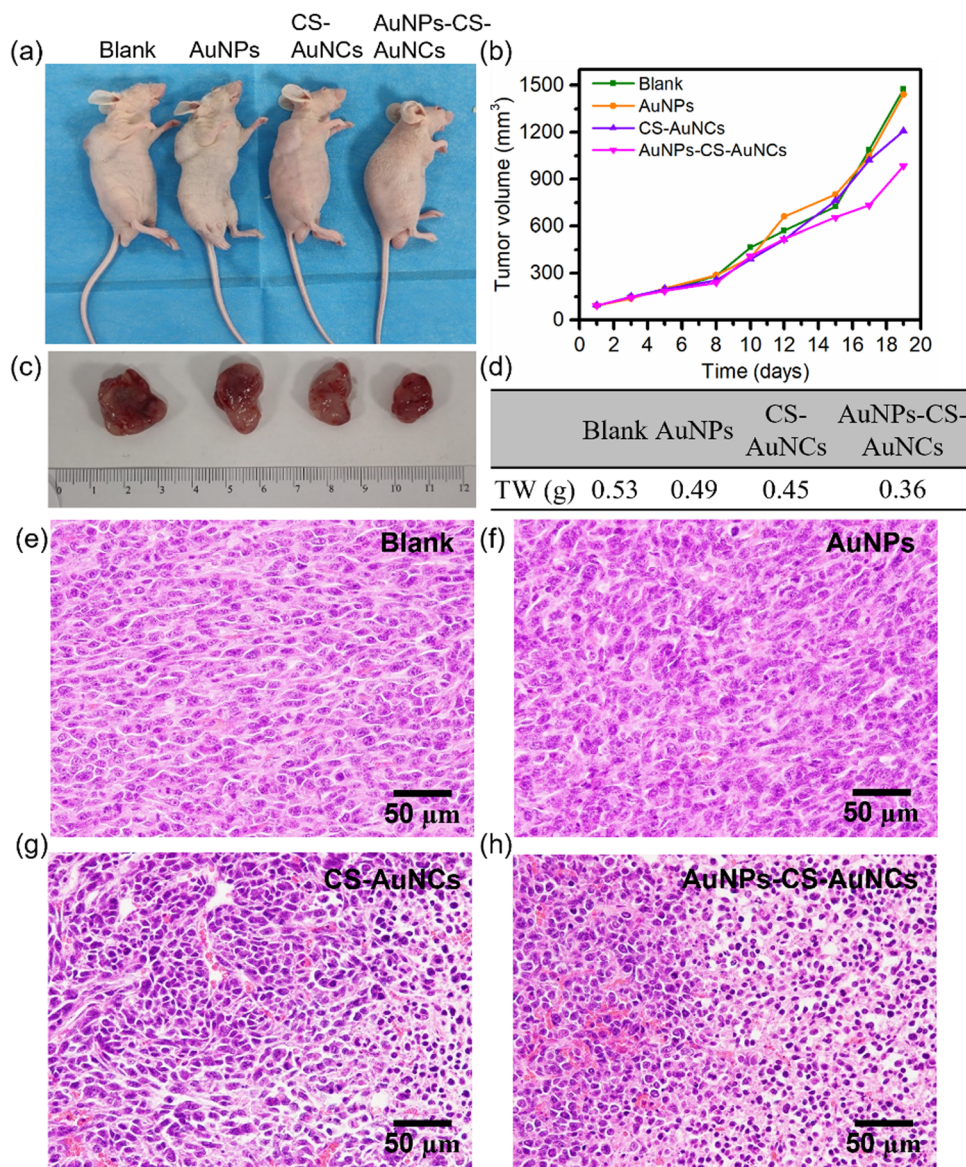
Fig. 6 (a) Photographs of HeLa-bearing mice after 19 days of the sample treatment under 5 min irradiation every four days. (b) Tumor growth curve of mice treated with different types of samples. (c) Photographs and (d) tumor weight of harvested tumors after the sample treatment. Tumor H&E staining of mice treated with samples of (e) PBS as a blank, (f) AuNPs, (g) CS-AuNCs and (h) AuNPs-CS-AuNCs.

than CS-AuNCs would be another reason. This also illustrates that the AuNPs-CS-AuNCs can be potentially used as an anti-cancer therapy agent with excellent antifouling properties and high photodynamic therapy efficiency; meanwhile, none of the other drugs need to be doped in. Therefore, the AuNPs-CS-AuNCs we prepared not only can sensitize the formation of singlet oxygen with high efficiency without the co-presence of any organic photosensitizer but also can maintain long circulation time and avoid being cleared quickly.

In vivo photodynamic therapy of our prepared gold nanocomposites was further investigated by the separate injection of PBS as a blank, AuNPs, CS-AuNCs and AuNPs-CS-AuNCs into HeLa tumor-bearing mice, and the mice were irradiated with white light for 5 min every four days. Then, the mice were sacrificed after 19 days of treatment (Fig. 6(a)). Similar tumor growth curves were observed for AuNP-treated mice and the control group, while the CS-AuNC treated group exhibited slight tumor growth inhibition after 19 days of treatment and the AuNPs-CS-AuNCs had the most significant tumor ablation with *ca.* 30% tumor weight inhibition and the tomour growth difference appeared after 10 days of treatment (Fig. 6(b)–(d)). In addition, as shown in Fig. 6(e)–(h), the H&E staining exhibited the most severe tumor damage for AuNPs-CS-AuNCs compared to the other groups. This result demonstrates that the AuNPs-CS-AuNCs with a core–shell structure has a much better photodynamic therapy efficiency with long blood circulation time than conventional gold nanoparticles or gold nanoclusters.

Conclusions

In summary, we designed a nanocomposite AuNPs-CS-AuNCs, with gold nanoparticles as the core and gold nanoclusters as the shell, which exhibited superior properties to normal AuNPs and AuNCs. AuNPs-CS-AuNCs of *ca.* 31 nm has higher fluorescence quantum yield and photodynamic efficiency than normal AuNCs, which is due to the higher cell penetration and surface plasmonic amplifying the photonic energy absorption and energy transfer from AuNPs in the core to neighboring AuNCs on the shell as demonstrated by *in vitro* and *in vivo* studies. Moreover, AuNPs-CS-AuNCs exhibited good colloidal stability and can have the ultra-low protein corona properties with potentially long blood circulation time by using protein casein as the AuNC preparation template, reducing agent and also as an antifouling agent. Our work opens a new avenue to design gold nanoclusters with high photodynamic therapy efficiency and ultra-low protein corona properties for anti-cancer therapy.

Conflicts of interest

There are no conflicts to declare.

Acknowledgements

References

1 C. T. Campbell, S. C. Parker and D. E. Starr, The effect of size-dependent nanoparticle energetics on catalyst sintering, *Science*, 2002, **298**, 811–814.

2 W. T. Wallace and R. L. Whetten, Coadsorption of Co and O_2 on selected gold clusters: Evidence for efficient room-temperature Co_2 generation, *J. Am. Chem. Soc.*, 2002, **124**, 7499–7505.

3 V. Poderys, G. Jarockyte, S. Bagdonas, V. Karabanovas and R. Rotomskis, Protein-stabilized gold nanoclusters for Pdt: Ros and singlet oxygen generation, *J. Photochem. Photobiol., B*, 2020, **204**, 111802.

4 X. Wu, L. Li, L. Zhang, T. Wang, C. Wang and Z. Su, Multifunctional spherical gold nanocluster aggregate@polyacrylic acid@mesoporous silica nanoparticles for combined cancer dual-modal imaging and chemo-therapy, *J. Mater. Chem. B*, 2015, **3**, 2421–2425.

5 R. Vankayala, C. L. Kuo, K. Nuthalapati, C. S. Chiang and K. C. Hwang, Nucleus-targeting gold nanoclusters for simultaneous *in vivo* fluorescence imaging, gene delivery, and nir-light activated photodynamic therapy, *Adv. Funct. Mater.*, 2015, **25**, 5934–5945.

6 T. Das, P. Ghosh, M. Shanavas, A. Maity, S. Mondal and P. Purkayastha, Protein-templated gold nanoclusters: Size dependent inversion of fluorescence emission in the presence of molecular oxygen, *Nanoscale*, 2012, **4**, 6018–6024.

7 P. Liu, W. Yang, L. Shi, H. Zhang, Y. Xu, P. Wang, G. Zhang, W. R. Chen, B. Zhang and X. Wang, Concurrent photothermal therapy and photodynamic therapy for cutaneous squamous cell carcinoma by gold nanoclusters under a single nir laser irradiation, *J. Mater. Chem. B*, 2019, **7**, 6924–6933.

8 L. Tang, X. Zeng, H. Zhou, C. Gui, Q. Luo, W. Zhou, J. Wu, Q. Li, Y. Li and Y. Xiao, Theranostic gold nanoclusters for nir-ii imaging and photodynamic therapy, *Chem. Res. Chin. Univ.*, 2021, **37**, 934–942.

9 J. Xie, Y. Zheng and J. Y. Ying, Protein-directed synthesis of highly fluorescent gold nanoclusters, *J. Am. Chem. Soc.*, 2009, **131**, 888–889.

10 Y. Wang, J.-T. Chen and X.-P. Yan, Fabrication of transferrin functionalized gold nanoclusters/graphene oxide nanocomposite for turn-on near-infrared fluorescent bioimaging of cancer cells and small animals, *Anal. Chem.*, 2013, **85**, 2529–2535.

11 J. Fan, R. Li, P. Xu, J. Di, Y. Tu and J. Yan, Sensitive sulfide sensor with a trypsin-stabilized gold nanocluster, *Anal. Sci.*, 2014, **30**, 457–462.

12 R. Ghosh, A. K. Sahoo, S. S. Ghosh, A. Paul and A. Chattopadhyay, Blue-emitting copper nanoclusters synthesized in the presence of lysozyme as candidates for cell labeling, *ACS Appl. Mater. Interfaces*, 2014, **6**, 3822–3828.

13 L. Nie, X. Xiao and H. Yang, Preparation and biomedical applications of gold nanocluster, *J. Nanosci. Nanotechnol.*, 2016, **16**, 8164–8175.

14 Y. Xu, J. Sherwood, Y. Qin, D. Crowley, M. Bonizzoni and Y. Bao, The role of protein characteristics in the formation

and fluorescence of Au nanoclusters, *Nanoscale*, 2014, **6**, 1515–1524.

15 K. Selvaprakash and Y.-C. Chen, Using protein-encapsulated gold nanoclusters as photoluminescent sensing probes for biomolecules, *Biosens. Bioelectron.*, 2014, **61**, 88–94.

16 J. Huang, L. Wang, R. Lin, A. Y. Wang, L. Yang, M. Kuang, W. Qian and H. Mao, Casein-coated iron oxide nanoparticles for high mri contrast enhancement and efficient cell targeting, *ACS Appl. Mater. Interfaces*, 2013, **5**, 4632–4639.

17 M. S. Bani, S. Hatamie and M. Haghpanahi, Biocompatibility and hyperthermia cancer therapy of casein-coated iron oxide nanoparticles in mice, *Polym. Adv. Technol.*, 2020, **31**, 1544–1552.

18 Y. N. Tan, J. Y. Lee and D. I. Wang, Uncovering the design rules for peptide synthesis of metal nanoparticles, *J. Am. Chem. Soc.*, 2010, **132**, 5677–5686.

19 Z. Zhong, S. Fang, Y. Li, Y. Huang, Y. Zhang, H. Chen, J. Zhang, H.-X. Wang, H. Xiong and Q. Zou, Quantitative analysis of protein corona on precoated protein nanoparticles and determined nanoparticles with ultralow protein corona and efficient targeting *in vivo*, *ACS Appl. Mater. Interfaces*, 2021, **13**, 56812–56824.

20 F. Chen, G. Wang, J. I. Griffin, B. Brenneman, N. K. Banda, V. M. Holers, D. S. Backos, L. Wu, S. M. Moghimi and D. Simberg, Complement proteins bind to nanoparticle protein corona and undergo dynamic exchange *in vivo*, *Nat. Nanotechnol.*, 2017, **12**, 387–393.

21 H. Yuan, J. Li, G. Bao and S. Zhang, Variable nanoparticle-cell adhesion strength regulates cellular uptake, *Phys. Rev. Lett.*, 2010, **105**, 138101.

22 J. Huang, L. Bu, J. Xie, K. Chen, Z. Cheng, X. Li and X. Chen, Effects of nanoparticle size on cellular uptake and liver mri with polyvinylpyrrolidone-coated iron oxide nanoparticles, *ACS Nano*, 2010, **4**, 7151–7160.

23 S.-H. Wang, C.-W. Lee, A. Chiou and P.-K. Wei, Size-dependent endocytosis of gold nanoparticles studied by three-dimensional mapping of plasmonic scattering images, *J. Nanobiotechnol.*, 2010, **8**, 1–13.

24 C. Cruje and B. Chithrani, Integration of peptides for enhanced uptake of pegylayed gold nanoparticles, *J. Nanosci. Nanotechnol.*, 2015, **15**, 2125–2131.

25 J. E. Zuckerman, C. H. J. Choi, H. Han and M. E. Davis, Polycation-sirna nanoparticles can disassemble at the kidney glomerular basement membrane, *Proc. Natl. Acad. Sci. U. S. A.*, 2012, **109**, 3137–3142.

26 E. C. Dreaden, L. A. Austin, M. A. Mackey and M. A. El-Sayed, Size matters: Gold nanoparticles in targeted cancer drug delivery, *Ther. Delivery*, 2012, **3**, 457–478.

27 A. H. Faraji and P. Wipf, Nanoparticles in cellular drug delivery, *Bioorg. Med. Chem.*, 2009, **17**, 2950–2962.

28 S. A. Kulkarni and S.-S. Feng, Effects of particle size and surface modification on cellular uptake and biodistribution of polymeric nanoparticles for drug delivery, *Pharm. Res.*, 2013, **30**, 2512–2522.

29 L.-Y. Zhang and T. Chu, Synthesis of composite particles with Fe_3O_4 core and ag shell for the development of fingerprints, *Bull. Korean Chem. Soc.*, 2013, **34**, 1457–1461.

30 X. Shi, D. Li, J. Xie, S. Wang, Z. Wu and H. Chen, Spectroscopic investigation of the interactions between gold nanoparticles and bovine serum albumin, *Chin. Sci. Bull.*, 2012, **57**, 1109–1115.

31 R. Herizchi, E. Abbasi, M. Milani and A. Akbarzadeh, Current methods for synthesis of gold nanoparticles, *Artif. Cells, Nanomed., Biotechnol.*, 2016, **44**, 596–602.

32 S. Singh, R. Kaur, J. Chahal, P. Devi, D. Jain and M. Singla, Conjugation of nano and quantum materials with bovine serum albumin (Bsa) to study their biological potential, *J. Lumin.*, 2013, **141**, 53–59.

33 M. Zhu, C. M. Aikens, F. J. Hollander, G. C. Schatz and R. Jin, Correlating the crystal structure of a thiol-protected Au25 cluster and optical properties, *J. Am. Chem. Soc.*, 2008, **130**, 5883–5885.

34 H. Zhao, X. Wen, W. Li, Y. Li and C. Yin, A copper-mediated on–off–on gold nanocluster for endogenous Gsh sensing to drive cancer cell recognition, *J. Mater. Chem. B*, 2019, **7**, 2169–2176.

35 I. O. Sosa, C. Noguez and R. G. Barrera, Optical properties of metal nanoparticles with arbitrary shapes, *J. Phys. Chem. B*, 2003, **107**, 6269–6275.

36 P. I. Haris and F. Severcan, Ftir spectroscopic characterization of protein structure in aqueous and non-aqueous media, *J. Mol. Catal. B: Enzym.*, 1999, **7**, 207–221.

37 G. Verma, N. G. Shetake, S. Pandrekar, B. Pandey, P. Hassan and K. Priyadarsini, Development of surface functionalized hydroxyapatite nanoparticles for enhanced specificity towards tumor cells, *Eur. J. Pharm. Sci.*, 2020, **144**, 105206.

38 S. Das, S. Mukhopadhyay, S. Chatterjee, P. S. Devi and G. Suresh Kumar, Fluorescent Zno–Au nanocomposite as a probe for elucidating specificity in DNA interaction, *ACS Omega*, 2018, **3**, 7494–7507.

39 Y. Yang, N. Gao, Y. Hu, C. Jia, T. Chou, H. Du and H. Wang, Gold nanoparticle-enhanced photodynamic therapy: Effects of surface charge and mitochondrial targeting, *Ther. Delivery*, 2015, **6**, 307–321.

40 P. G. Calavia, G. Bruce, L. Pérez-García and D. A. Russell, Photosensitiser-gold nanoparticle conjugates for photodynamic therapy of cancer, *Photochem. Photobiol. Sci.*, 2018, **17**, 1534–1552.